Eur Radiol (2008) 18: 1018–1023
DOI 10.1007/s00330-007-0834-4

M. Viallon
M. I. Vargas
H. Jlassi
K. O. Lövblad
J. Delavelle

High-resolution and functional magnetic resonance imaging of the brachial plexus using an isotropic 3D T2 STIR (Short Term Inversion Recovery) SPACE sequence and diffusion tensor imaging

Received: 27 July 2007
Revised: 19 October 2007
Accepted: 27 November 2007
Published online: 8 January 2008

M. Viallon (✉) · M. I. Vargas ·
H. Jlassi · K. O. Lövblad · J. Delavelle
Department of Radiology,
University Hospital of Geneva,
Rue Micheli du Crest, 24,
1211 Geneva, Switzerland
e-mail: magalie.viallon@hcuge.ch
Tel.: +41-22-3725209
Fax: +41-22-3727072

Abstract This technical note demonstrates the relevance of the isotropic 3D T2 turbo-spin-echo (TSE) sequence with short-term inversion recovery (STIR) and variable flip angle RF excitations (SPACE: Sampling Perfection with Application optimized Contrasts using different flip angle Evolutions) for high-resolution brachial plexus imaging. The sequence was used in 11 patients in the diagnosis of brachial plexus pathologies involving primary and secondary tumors, and in six volunteers. We show that 3D STIR imaging is not only a reliable alternative to 2D STIR imaging, but it also better evaluates the anatomy, nerve site compression and pathology of the plexus, especially to depict space-occupying tumors along its course. Finally, due to its appropriate contrast we describe how 3D-STIR can be used as a high-resolution mask to be fused with fraction of anisotropy (FA) maps calculated from diffusion tensor imaging (DTI) data of the plexus.

Keywords Brachial plexus · Magnetic resonance · Three-dimensional · STIR · DTI

Introduction

Brachial plexus examination remains difficult because of its particular orientation and is conventionally realized using sequential multiplanar 2D sequences with various contrasts such as T1, T2 and T2 STIR sequences for fat saturation contrast [1–4]. As a consequence, the acquisition plane is never exactly the right plane to better visualize and analyze the brachial plexus. Three-dimensional acquisitions allow one to reconstruct images either perpendicular to the plexus, or in double obliquity, to slice through the complete plexus, and they play an important role in defining the site and etiology of the nerve compression. But until recently, 3D acquisitions implemented to image the plexus were highly T2 weighted, like CISS3D or TrueFISP3D sequences [5, 6]. The clinical relevance of these 3D sequences was especially demonstrated when cerebrospinal fluid (CSF) is involved: compressive nerve roots and nerve roots avulsions are very well depicted due to the strong T2 myelographic contrast between nerves and fluid provided by these sequences [5]. Nevertheless, to study the whole course of the plexus, a fat-saturated T2 sequence with an inversion recovery excitation is necessary and offers a more adequate contrast of trunks and cords [7]. This paper investigates the feasibility of 3D STIR imaging of the brachial plexus using an inversion recovery (IR) 3D TSE sequence with variable flip angle RF excitations (SPACE: Sampling Perfection with Application optimized Contrasts using different flip angle Evolutions) [8] and its clinical relevance in various pathologies of the brachial plexus.

Materials and methods

Eleven patients and six volunteers were examined on a 1.5-T Avanto MRI scanner (Siemens, Erlangen, Germany) with respect to approval by the local ethics committee and the Stockholm chart. The six-element body-array coils were combined with the three elements of the posterior part of the neck array coil, six elements of the head array coils and three elements of the spine array coils to cover the FOV with 18 coil elements.

The 3D SPACE sequence [8] was modified to include an IR magnetization preparation with TI=160 ms for fat saturation contrast. Parallel acquisition (iPAT factor=3), and variable flip angles along the echo train were used. Each 3D STIR acquisition consists of a large coronal slab with around 96 partitions centered on the brachial plexus. The isotropic voxel size was 0.9 to 1 mm^3. MR parameters were: TE=149 ms, TR=2,000 ms, TI=160 ms, turbofactor=73, TA=6–7 min, FOV=256, matrix size=256×260. The acquisition time varied between 6 to 9 min depending on the desired spatial coverage (number of slices ≥96). The sequence can be implemented with or without flow compensation, but in order to achieve the large mandatory spatial coverage in relatively short acquisition time, the sequence was rather not flow compensated. In such a case, it would not be relevant to analyze the spinal cord. The acquisition plane was coronal, with a right-left phase encoding direction. For each patient, thin maximum intensity projection (MIP) and multiplanar reconstruction reformatted coronal, coronal oblique and curvilinear through the plexus from right to left were obtained from the same 3D dataset. The slice thickness of the thin MIP was between 3 to 5 mm; the reconstruction was interleaved every 1 mm.

The diffusion tensor images were acquired in the axial plane with the following MR parameters: TE=92 ms, TR=9,000 ms, iPAT=2, Nex 1; FOV 230, matrix 128×128, slice thickness 2 mm resulting in a voxel size of 2×2×2 mm, b values=0 and 900 s/mm^2, and 30 gradient directions. The DTI sequence duration was 5 min 44 s. FA, ADC maps and tensor calculation were performed in-line by the MRI scanner.

The 3D datasets were analyzed using either the 3D Syngo (Siemens, Germany) task card (for simple MPR and MIP reconstruction on the 3D-STIR dataset) or using the Neuro3D Syngo software (for fusion with fraction of anisotropy (FA) maps calculated from the DTI dataset of the plexus or fiber tracking). Fiber tracks of the brachial plexus are calculated using a fourth order Runge-Kutta algorithm from several seed points placed at different levels of the spinal cord close to the nerves roots. Prior to tracking a spatial filter (FWHM=5 mm) is applied to the data for noise reduction purposes.

Results

Demographic data of the study population are shown in Table 1. The subjects ranged in age between 16 and 80. Three patients had primary tumors, two neurogenic brachial plexus tumors and one primary pleural tumor (patients 1, 2, and 3); four patients had secondary tumors (patients 4–7), and four patients were normal (patients 8–11).

In all volunteers and patients, the brachial plexus was clearly identified on the 3D STIR sequence. The normal brachial plexus appears in discrete hyper signal on the fat-

Table 1 Demographic data of the study population

	Age/sex	Pathology	Findings
1	28/M	Multiple schwannomas	Fibers surrounding tumor
2	42/F	Schwannoma C5	Enlargment C5
3	59/M	Desmoblastic mesothelioma	Displacement C8
4	64/F	Pancoast	Infiltration right brachial plexus
5	80/M	Esophagueal adenocarcinoma	Metastasis C1 and first costal rib
6	77/F	Breast cancer metastasis	Infiltration in C7
7	57/M	Lymphoma	Perineural infiltration C7-C8
8	16/F	Normal	Normal
9	31/M	Normal	Normal
10	45/F	Normal	Normal
11	69/F	Normal	Normal
Control 1	38/M	Normal	Normal
Control 2	41/M	Normal	Normal
Control 3	38/M	Normal	Normal
Control 4	31/M	Normal	Normal
Control 5	20/M	Normal	Normal
Control 6	40/F	Normal	Normal

*All pathologies have been biopsy proven

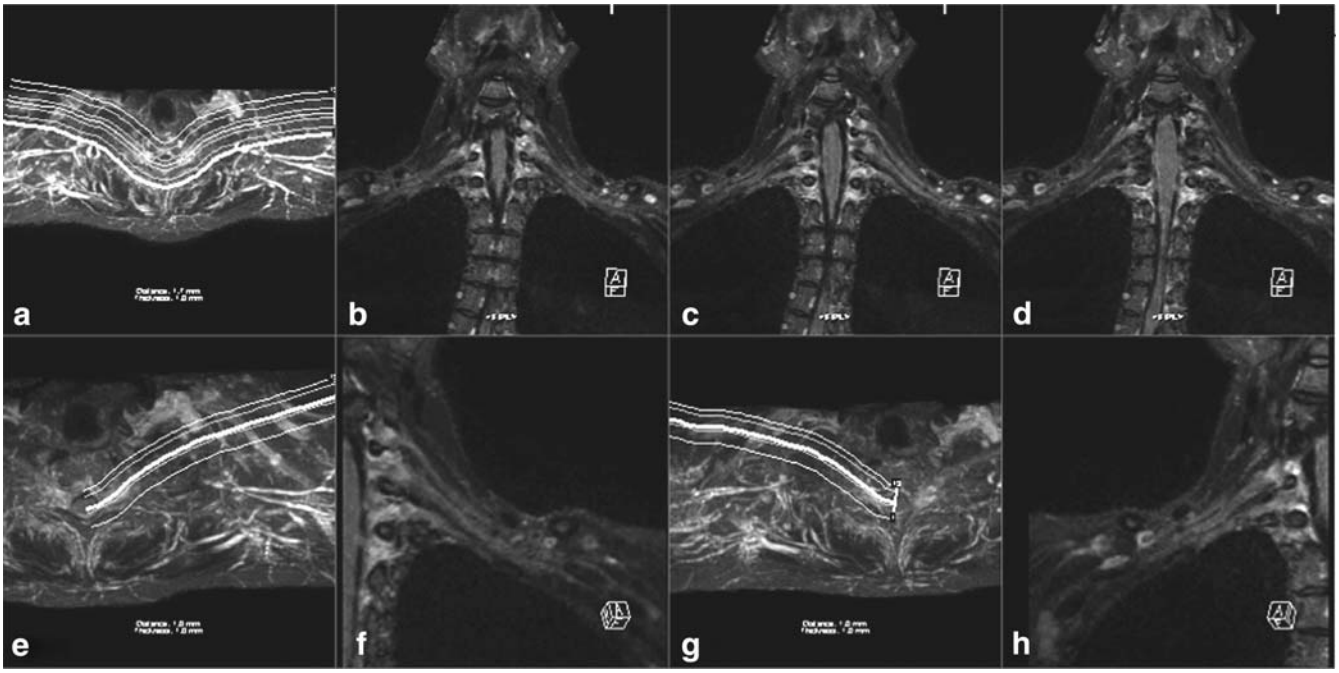

Fig. 1 Normal control: **a**, **e**, **g**: topograms, **b**–**d**: curved MPR. **f** and **h**: Coronal oblique MPR reconstruction for left and right brachial plexus, respectively. The white lines indicate the plane corresponding to the MPR images. Note how the brachial nerve anatomy is very well rendered and how the 3D volume acquisition helps to see the relationship with local background

suppressed background signal, whereas the primary and secondary tumors appear in clear hyper signal along the nerves.

Good image quality was obtained in all our patients. We could display the plexus using curved or oblique MPR as well as thin MIP: one example is given in Fig. 1 on a normal subject. In all brachial plexuses, we could reliably reconstruct the nerve course from the spinal cord to the distal area, and especially we had a good evaluation of the supraclavicular region. In patient 5, the lesions shown in Fig. 2 were missed using the standard 2D protocol, consisting of localized sagittal and coronal 2D STIR sequences, due to the limited number of slices. These lesions were identified on the 3D STIR acquisition due to the large and complete coverage of the brachial plexus. The technique appears very important for surgical and oncologic planning as it is possible to differentiate deformation (Figs. 3 and 4) from infiltration (Fig. 5).

Finally, 3D STIR can be used as a high-resolution mask to be fused with fraction of anisotropy (FA) maps calculated from diffusion tensor imaging (DTI) data (Fig. 4).

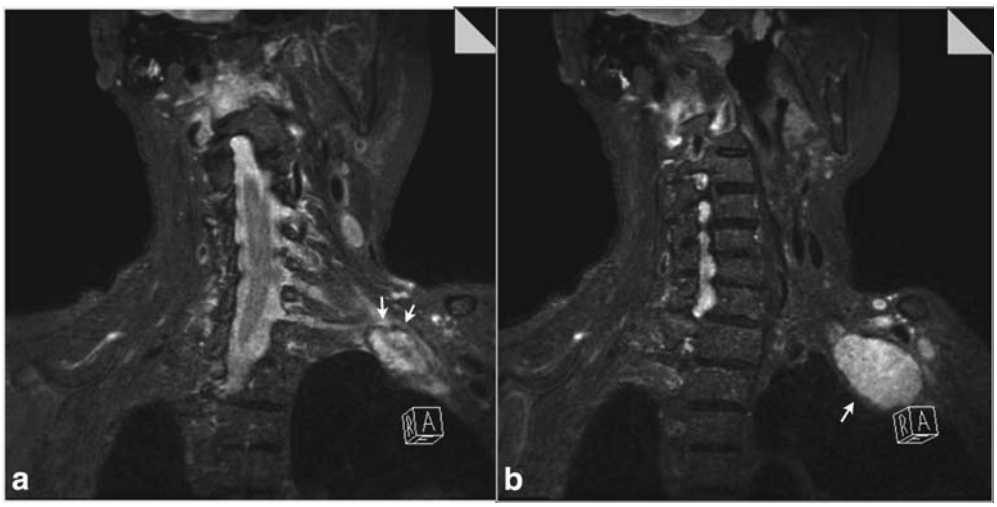

Fig. 2 Case 5: coronal oblique reconstruction of left brachial plexus shows displacement of the inferior trunk (arrow on **a**) by an esophageal metastasis of the first rib (arrowhead on **b**)

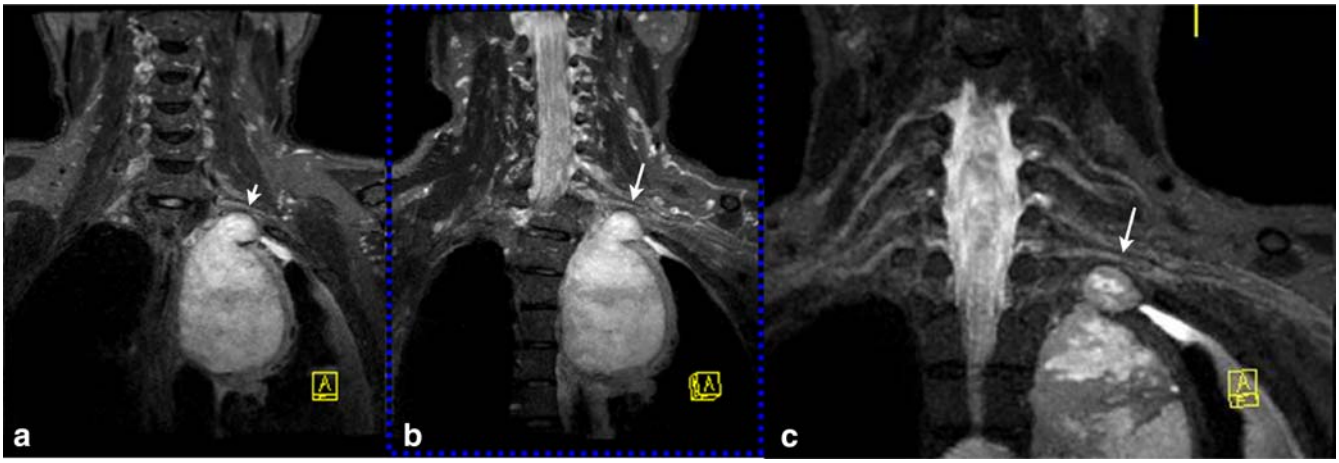

Fig. 3 Case 3: coronal MPR (**a**), curved coronal oblique MPR (**b**), curved thin MIP 5 mm (**c**) slicing through right and left plexus show well-delineated displacement of the C8 root (arrow) by a desmoblastic mesothelioma

In Fig. 3, note how the fibers are spread over by the tumors and how their course surrenders the lesions. Both the 3D STIR images and the DTI fiber tracking evidence a deformation of the brachial plexus due to the tumor.

Fiber tracks of the plexus were nicely obtained in six of ten patients; in four patients it was not possible to calculate them due to insufficient image quality resulting from motion artifacts and noise.

Discussion

High-quality MR neurography of the brachial plexus is possible using the 3D-STIR sequence; the nerve are clearly visualized. 3D-STIR sequence demonstrates better capacity than conventional 2D acquisitions to depict anatomy and lesions of the brachial plexus and to identify the number of lesions, but also to analyze their spatial extension within and along the nerve tracts. The anatomical coverage offered by the 3D acquisition and the ability to slice through the volume of interest help to analyze how the lesion modifies and impacts the nerves course. It can be very useful in the tumoral pathology since nerve distortion and/or compression caused by the lesions can be nicely displayed by MIP and MPR. 3D imaging of complex nerve entrapment and compression syndrome of the brachial plexus clearly help the analysis, the detection of compression sites, and the characterization of space-occupying lesions.

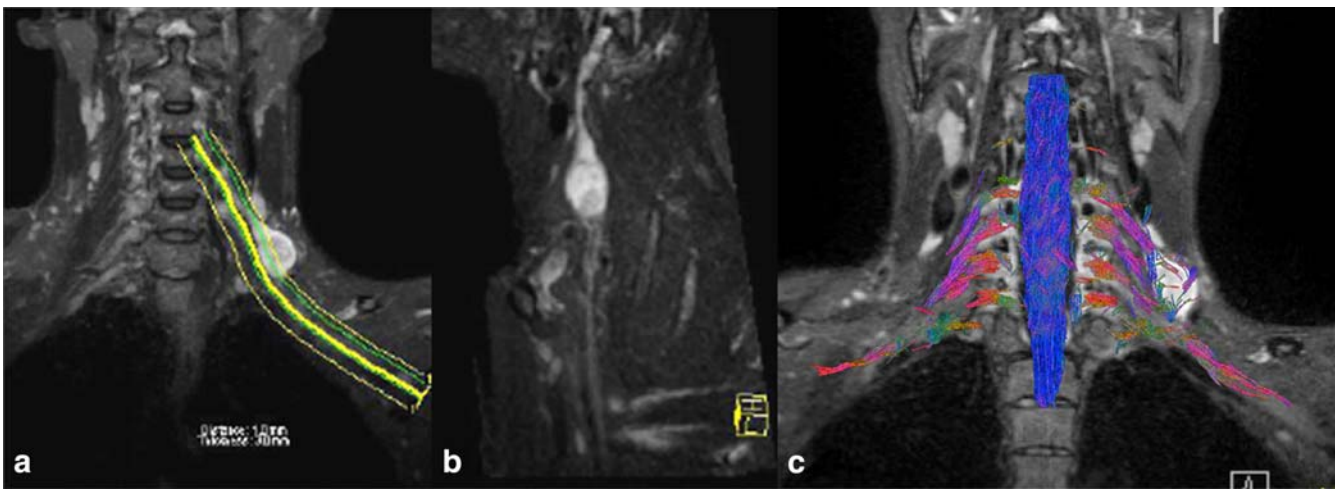

Fig. 4 Case 2: coronal 3D STIR and superimposed topogram (**a**) corresponding to the thin curved MPR reconstruction; **b** displays the results of the MPR reconstruction along the nerve tracts, showing nicely the enlargement of the C5 root by the schwannoma. (**c**): 3D STIR used as a high resolution mask to be fused with the fiber tracts calculated from diffusion tensor imaging (DTI); the image displays the fiber tracts in color-coded map superimposed on the anatomical STIR 3D images. Note the clear spreading out of the fibers along the tumor

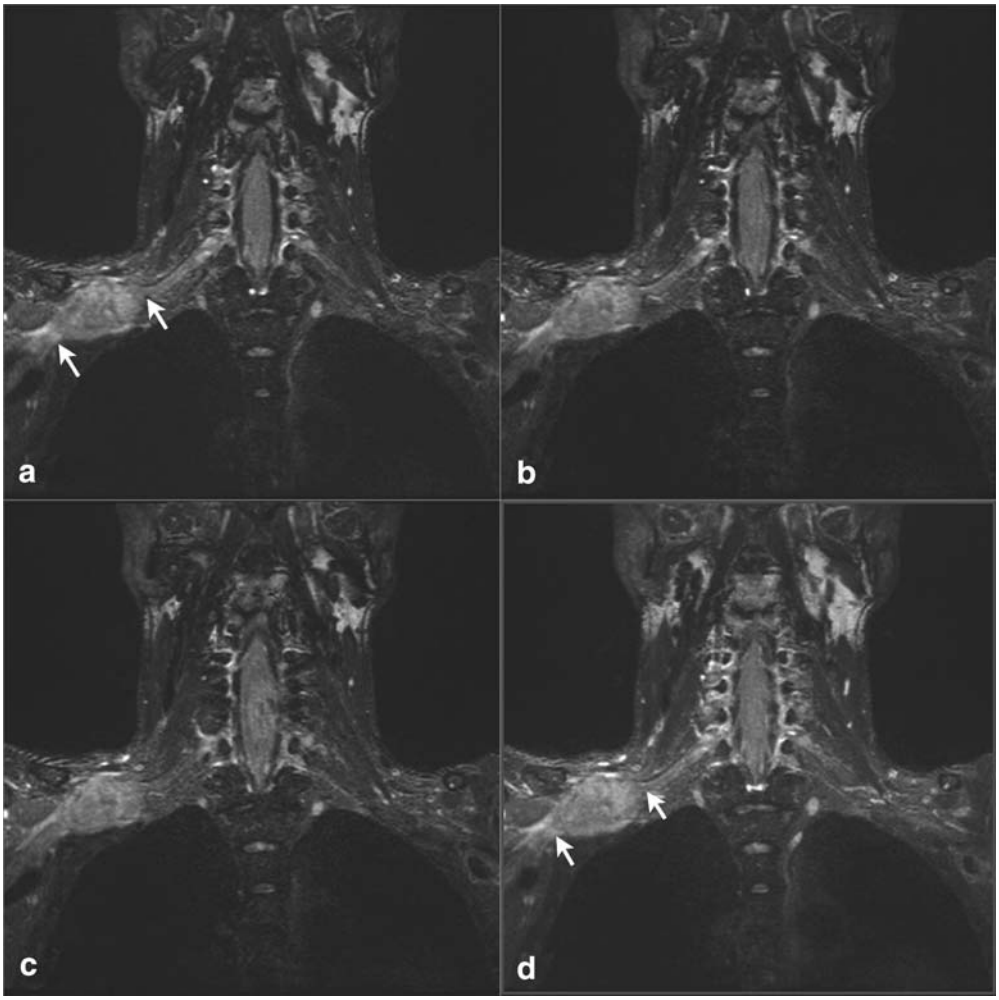

Fig. 5 Case 7: thin MPR (**a**–**c**) and MIP (**d**) reconstructions show the lesion with perineural dissemination in case of systemic lymphoma (arrow)

The sequence also allows one to analyze the bone marrow contrast similarly to 2D-STIR and is adequate for musculoskeletal examination. To achieve the large spatial coverage in short acquisition time, the sequence is not flow compensated, and in such configuration it is not relevant to analyze the spinal cord due to flow artifacts. For traumatic injuries involving the spinal cord, such as nerve avulsion, for example, the sequence may be useful if it is flow compensated or if the acquisition plane is set perpendicular to the cerebral spinal fluid (CSF) flow. Nevertheless, it will result in an increased acquisition time that may restrain the use of the sequence to localized examination.

The motivation for 3D STIR was also to provide a nice, appropriate 3D background for anatomical fusion with fiber tracts of the complete plexus nerves. Several studies have reported the use of DTI to image the spinal cord [9–12], but not in the brachial plexus. We demonstrate here that DTI with fiber tracking reconstruction can demonstrate nerve tracts and their alterations or deformation due to pathological processes located surrounding or along the brachial plexus. The reliability of the DTI sequence is nevertheless strongly dependent on the corpulence of the patient, with a severely degraded image quality on plethoric patients.

Conclusions

We found 3D SPACE STIR acquisition without flow compensation to be very useful for the initial screening of patients with tumoral etiologies of the brachial plexus. It is a valuable adjunct in the detection of space-occupying lesions where it may improve quantification of lesions, yield better depiction of nerve site compression and ultimately provide a better understanding of the pathophysiology.

Acknowledgment The authors thank Stefan Huwer and Heiko Maïer from the Siemens Advanced Neuro MR Development Group in Erlangen for helpful discussions and collaboration on the Neuro3D software.

References

1. Aagaard BD, Maravilla KR, Kliot M (1998) MR neurography MR imaging of peripheral nerves. Magn Reson Imaging Clin N Am 6(1):179–194
2. Kim S et al (2007) Role of magnetic resonance imaging in entrapment and compressive neuropathy-what, where, and how to see the peripheral nerves on the musculoskeletal magnetic resonance image: part 2. Upper extremity. Eur Radiol 17(2):509–522
3. Todd M, Shah GV, Mukherji SK (2004) MR imaging of brachial plexus. Top Magn Reson Imaging 15(2):113–125
4. van Es HW (2001) MRI of the brachial plexus. Eur Radiol 11(2):325–336
5. Gasparotti R et al (1997) Three-dimensional MR myelography of traumatic injuries of the brachial plexus. AJNR Am J Neuroradiol 18(9):1733–1742
6. Vargas MI et al (2007) Clinical applications of diffusion tensor tractography of the spinal cord. Neuroradiology. Oct 2; [Epub ahead of print] DOI 10.1007/s00234-007-0309-y
7. Zhou L, Yousem DM, Chaudhry V (2004) Role of magnetic resonance neurography in brachial plexus lesions. Muscle Nerve 30(3):305–309
8. Lichy MP et al (2005) Magnetic resonance imaging of the body trunk using a single-slab, 3-dimensional, T2-weighted turbo-spin-echo sequence with high sampling efficiency (SPACE) for high spatial resolution imaging: initial clinical experiences. Invest Radiol 40(12):754–760
9. Ducreux D et al (2005) Brain MR diffusion tensor imaging and fibre tracking to differentiate between two diffuse axonal injuries. Neuroradiology 47(8):604–608
10. Liberatore M et al (2006) Diffusion tensor imaging and tractography of central pontine myelinolysis. J Neuroradiol 33(3):189–193
11. Roze E et al (2007) Propriospinal myoclonus: Utility of magnetic resonance diffusion tensor imaging and fiber tracking. Mov Disord 22 (10):1506–1509
12. Schwartz ED et al (2005) Spinal cord diffusion tensor imaging and fiber tracking can identify white matter tract disruption and glial scar orientation following lateral funiculotomy. J Neurotrauma 22(12):1388–1398